

Manipulating Hydrocarbon Chain-Melting Transitions in Dialkylammonium Halide Barocaloric Materials through Desymmetrization

Faith E. Chen, Jason D. Braun, Jinyoung Seo, Hailey J. Hurd, Malia B. Wenny, Shao-Liang Zheng, Jason J. Calvin, Craig M. Brown, and Jarad A. Mason*



Cite This: *J. Am. Chem. Soc.* 2025, 147, 19788–19795



Read Online

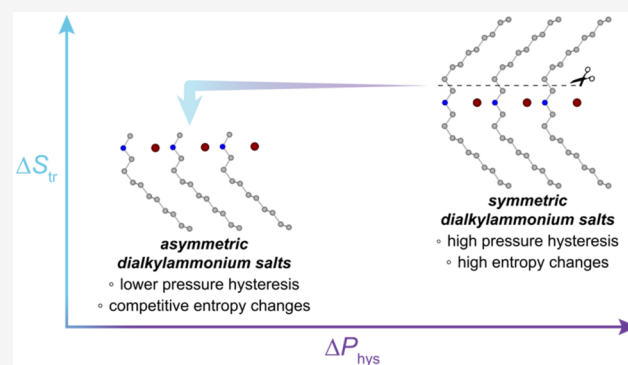
ACCESS |

Metrics & More

Article Recommendations

Supporting Information

ABSTRACT: Layered materials containing hydrocarbon bilayers capable of transitioning between an ordered and partially disordered state can exhibit large temperature and entropy changes—termed barocaloric effects—in response to a change in hydrostatic pressure. These barocaloric materials can, in principle, be used to drive heating and cooling cycles with higher efficiency and less environmental impact than conventional fluorocarbon refrigerants. However, much remains to be understood about how to manipulate the thermodynamics and kinetics of hydrocarbon order–disorder, or “chain-melting”, transitions in the solid state in order to design materials with properties tailored for specific thermal applications. Here, we report a chain desymmetrization strategy to modulate the phase-change behavior of a new family of asymmetric dialkylammonium halide salts. In particular, we demonstrate that chain desymmetrization can lead to reduced phase-change thermal hysteresis while maintaining large entropy changes. This translates to a significant reduction in the pressure required to reversibly drive nonzero entropy changes, with asymmetric dialkylammonium salts able to access reversible entropy changes at pressures nearly 80% lower than their symmetric counterparts. This work expands the scope of chain-melting materials that exhibit strong barocaloric effects and offers insights into the factors that influence the reversibility of barocaloric materials.



INTRODUCTION

Barocaloric materials—solids that undergo thermal changes in response to applied hydrostatic pressure—have the potential to serve as sustainable refrigerants that circumvent many of the environmental and safety pitfalls associated with conventional volatile refrigerants.^{1–5} In effective barocaloric materials, large thermal changes are induced when the application or removal of pressure drives a first-order phase transition—typically between a more ordered and a more disordered state.⁶ Changes in accessible degrees of freedom between the two states manifest as an entropy change that, in concert with other factors such as thermal conductivity and heat capacity, determines the amount of heat that can be moved by cycling through the transition. High-performance barocaloric materials can access entropy changes that approach those of state-of-the-art hydrofluorocarbon (HFC) and hydrofluoroolefin (HFO) refrigerants on a gravimetric basis and exceed them on a volumetric basis.^{7–9}

In pursuit of barocaloric materials that feature large entropy changes, solid-state hydrocarbon disordering (often termed “chain-melting”) transitions have emerged as a particularly promising mechanism. In chain-melting processes, aliphatic chains reversibly transition between a densely packed, ordered

phase and a partially disordered phase, wherein individual chains sample various rotational and vibrational degrees of freedom while confined in the solid-state.^{10,11} Entropy changes of up to $300 \text{ J kg}^{-1} \text{ K}^{-1}$ ($320 \text{ J L}^{-1} \text{ K}^{-1}$) are accessible through these types of transitions, as recently demonstrated in two classes of materials with hydrocarbon bilayer-type structures: hybrid organic–inorganic perovskites^{12,13} and dialkylammonium halide salts.^{14,15}

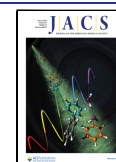
To fully harness the potential of chain-melting transitions for thermal applications, it is critical to be able to manipulate the transition behavior in a predictable fashion. Both hybrid organic–inorganic perovskites and dialkylammonium halide salts are highly tunable classes of barocaloric materials, allowing chain-melting transitions to, in principle, be modulated by adjusting inter/intralayer interactions through

Received: March 2, 2025

Revised: May 8, 2025

Accepted: May 13, 2025

Published: May 30, 2025



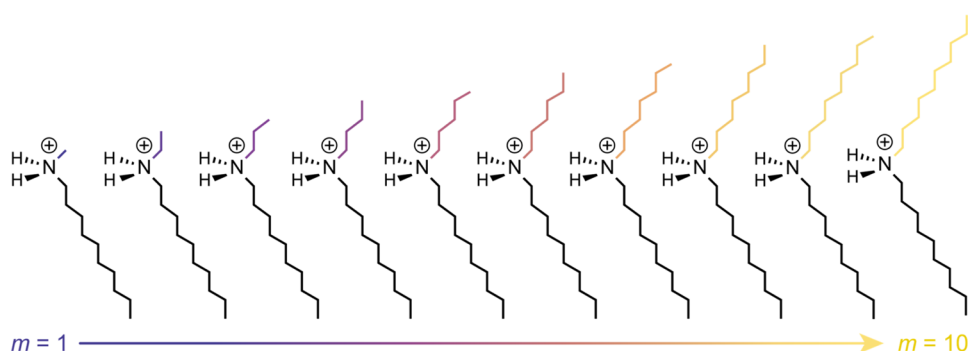


Figure 1. ChemDraw representations of C_mC_{10} cations for the series of dialkylammonium bromide ($C_mC_{10}\text{-Br}$) salts studied in this work. For a given C_mC_{10} cation, m refers to the length of the n -alkyl substituent opposite the fixed n -decyl substituent.

the use of different hydrocarbon species and anions. Efforts to investigate how such modifications affect chain-melting behavior, however, are currently in their infancy. For instance, with hybrid organic–inorganic perovskites, most research has focused on understanding the effects of structural and chemical modifications on optoelectronic performance^{16,17} rather than phase change thermodynamics and kinetics.¹⁸ Meanwhile, for the more nascent class of barocaloric dialkylammonium salts, reports on chain-melting behavior are currently limited to anion-driven effects.^{14,19–22}

Here, we report a systematic study of how desymmetrization of dialkylammonium salts impacts their thermal properties and barocaloric performance. Specifically, we manipulate the length of alkyl substituents on dialkylammonium cations relative to one another and characterize the resulting changes in phase transition behavior through calorimetric and structural studies. In so doing, we discover a subset of asymmetric dialkylammonium salts that consistently display highly reversible barocaloric behavior—by way of reduced thermal hysteresis—while retaining large gravimetric entropy changes. Ultimately, through this work, we expand the library of barocaloric materials that undergo chain-melting transitions and establish insights that advance progress toward the precise and controllable design of sustainable, solid refrigerants.

RESULTS AND DISCUSSION

Dialkylammonium salts are a family of organic, chain-melting materials with exceptional promise for barocaloric applications, owing to their large entropy changes, high stability, and solution processability.^{14,15,22} In these soft materials, dialkylammonium cations assemble into layered structures—reminiscent of phospholipid bilayers in cell membranes—through charge-assisted hydrogen bonding interactions with different anions. The charge-balancing anion is readily exchangeable through anion metathesis or acid–base chemistry, and consequently, efforts thus far to modulate transition behavior in dialkylammonium salts have focused on anion tuning. In particular, certain anion properties (e.g., size, polarizability) have been hypothesized, and shown in some cases, to influence chain confinement and, by extension, chain-melting.^{14,21}

Manipulating chain confinement through anion selection is a viable, albeit indirect, strategy for controlling chain-melting behavior. Moreover, with anion modulation, it remains challenging to decrease hysteresis while maintaining a large entropy change and sharp transition.^{14,21} Alteration of the aliphatic chains themselves, on the other hand—for instance

through truncation or elongation of chain length, installation of functional groups, or introduction of chain branching—could offer an alternative, more direct approach for manipulating chain-melting processes. Promisingly, analogous chain-melting (“gel–fluid”) transitions in phospholipid bilayers are known to show highly variable behavior when phospholipids with identical alkyl chain lengths are exchanged for those with nonidentical chains.²³ As such, we hypothesized that introducing chain length dissimilarity in dialkylammonium salts could provide a straightforward way to access new phase-change behavior and establish useful insights into chain-melting—and, by extension, barocaloric—behavior.

Synthesis of Asymmetric Dialkylammonium ($C_mC_{10}\text{-Br}$) Salts. To investigate the effect of chain length dissimilarity on the chain-melting behavior of dialkylammonium salts, we prepared a series of dialkylamines wherein one alkyl substituent is fixed in length at ten carbons while the other varies between one and ten (Figure 1). We herein refer to these amines as C_mC_{10} , where m denotes the length of the varying alkyl substituent opposite the fixed decyl group. Conveniently, all C_mC_{10} amines in this work can be prepared through a generalizable procedure consisting of a sodium methoxide-catalyzed amide coupling followed by reduction to the amine. Following preparation of C_mC_{10} amines, $C_mC_{10}\text{-Br}$ salts can be obtained through acidification of the appropriate amine with hydrobromic acid. We selected bromide as the charge-balancing anion for all salts to ensure that any changes in transition behavior could be ascribed solely to chain length effects, as well as to favor higher transition temperatures which simplify structural characterization (*vide infra*).

The identities of synthesized $C_mC_{10}\text{-Br}$ salts were confirmed using ^1H and ^{13}C nuclear magnetic resonance (NMR) spectroscopy (Supporting Information Section 2), high-resolution mass spectrometry (Supporting Information Section 2), X-ray crystal structures where possible (Supporting Information Section 3), powder X-ray diffraction (Supporting Information Section 3), and thermogravimetric analysis (Supporting Information Section 4).

Chain-Melting in Asymmetric Dialkylammonium ($C_mC_{10}\text{-Br}$) Salts. To characterize the thermal phase transition behavior of $C_mC_{10}\text{-Br}$ salts, we performed differential scanning calorimetry (DSC) experiments between 198 and 473 K (Figures S72–S80). All $C_mC_{10}\text{-Br}$ salts were observed to undergo reversible, solid–solid transitions between 225 and 375 K (Figure 2). Interestingly, the observed transition temperatures follow an unexpected trend with increasing m chain length, or increasing chain length similarity.

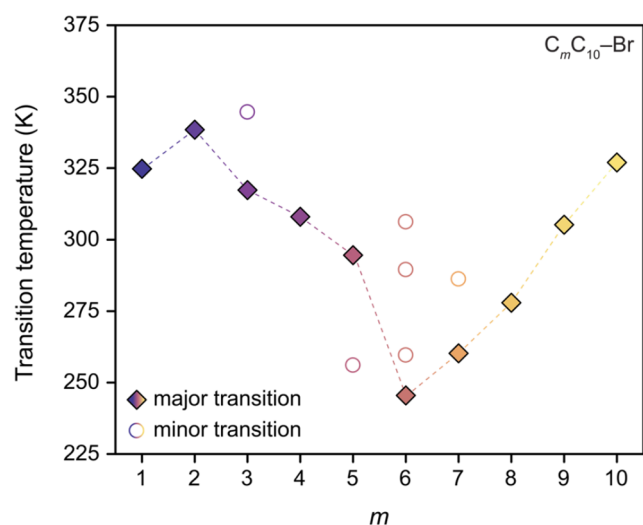


Figure 2. Chain-melting transition temperatures for $C_m C_{10}\text{-Br}$ salts recrystallized from methanol obtained using a scan rate of 2 K/min. Filled diamonds and hollow circles denote the major and minor (if present) transition(s), respectively, for a given $C_m C_{10}\text{-Br}$ salt. The major transition was defined as the transition exhibiting the largest entropy change. The dashed line illustrates the trend in major transition temperatures across the series. Uncertainties in temperature are smaller than the size of the data points.

At low m values and low chain length similarities, $C_1 C_{10}\text{-Br}$ and $C_2 C_{10}\text{-Br}$ undergo single chain-melting transitions at 324 and 338 K, respectively. These transition temperatures are similar to the previously reported, symmetric $C_{10} C_{10}\text{-Br}$ salt, which undergoes a chain-melting transition at 327 K. However, as m increases to salts with more intermediate chain length similarities ($C_3 C_{10}\text{-Br}$ through $C_7 C_{10}\text{-Br}$), chain-melting behavior is fragmented into as many as four transitions—apart from $C_4 C_{10}\text{-Br}$, which maintains a single transition—and a significant depression in transition temperatures is observed to as low as 245 K. Further increase of m to salts with higher chain length similarities ($C_8 C_{10}\text{-Br}$ and $C_9 C_{10}\text{-Br}$) is accompanied by the reappearance of single chain-melting transitions and increased transition temperatures.

The caldera-like behavior observed in the $C_m C_{10}\text{-Br}$ series does not resemble the trends encountered in typical n -alkyl-containing systems (such as fatty acids²⁴ and n -alkanes^{25,26}), where increasing chain length is often accompanied by monotonic or staggered increases in transition temperature. Instead, the phase-change behavior of $C_m C_{10}\text{-Br}$ salts more closely resembles that of mixed-chain phospholipids with two acyl chains of differing length or functional groups.²⁷ Indeed, studies on aqueous dispersions of saturated, mixed-chain phosphatidylcholines [$C(n_1)C(n_2)PC$] (n_1 = length of acyl chain 1, n_2 = length of acyl chain 2, PC = phosphatidylcholine) have similarly found that the chain-melting transition temperature follows an inverted, bell-shaped curve with respect to chain similarity.²⁸ In these systems, mixed-chain phosphatidylcholines of very high and very low chain similarities display higher transition temperatures than phosphatidylcholines with intermediate chain similarities. X-ray diffraction^{29,30} and vibrational spectroscopy^{31–33} studies suggest that this trend results from chains adopting different packing arrangements—dictated by the extent of mismatch between chain lengths—to maximize van der Waals contacts.

Structural Insight into Asymmetric Dialkylammonium ($C_m C_{10}\text{-Br}$) Salts. To investigate whether chain packing effects were similarly operative in the $C_m C_{10}\text{-Br}$ series, we sought to gain structural insight into the ordered and disordered phases of $C_m C_{10}\text{-Br}$ salts. However, single-crystal X-ray diffraction structures were only obtainable for the ordered, low-temperature phases of $C_1 C_{10}\text{-Br}$, $C_2 C_{10}\text{-Br}$, and $C_9 C_{10}\text{-Br}$. In all other cases, extensive twinning and disorder prevented structural determination.

Crystal structures for $C_1 C_{10}\text{-Br}$, $C_2 C_{10}\text{-Br}$ and $C_9 C_{10}\text{-Br}$ collected at 100 K reveal that the alkyl chains on the asymmetric dialkylammonium cations pack in a noninterdigitated, end-to-end fashion. The salt with the greatest mismatch in chain lengths, $C_1 C_{10}\text{-Br}$, crystallizes into the monoclinic space group $P2_1$ and displays uniform packing of its [$C_1 C_{10}$]⁺ cations throughout the structure, with C_1 portions on one cation aligned with C_1 portions on neighboring cations (Figure 3a). Consequently, the C_{10} chains pack exclusively with C_{10} chains on neighboring cations and interact exclusively with C_{10} chain ends from the next layer of cations. $C_1 C_{10}\text{-Br}$ thus adopts an ordered layered structure where short chains pack

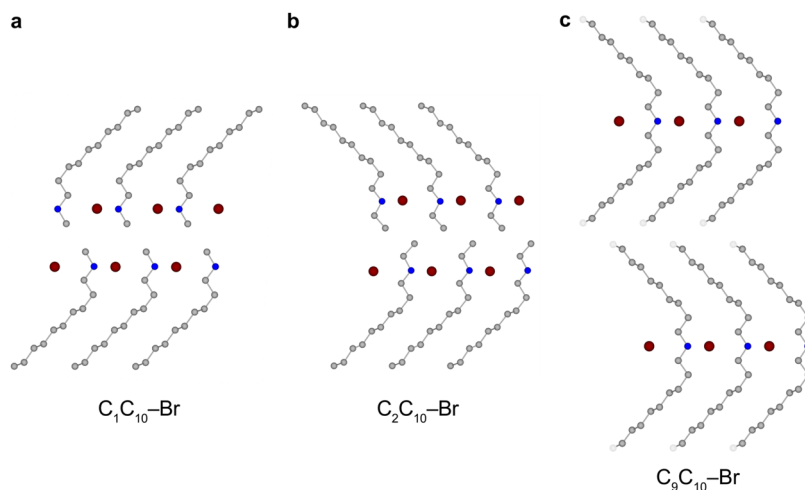


Figure 3. 100-K single-crystal structures of (a) $C_1 C_{10}\text{-Br}$, (b) $C_2 C_{10}\text{-Br}$, and (c) $C_9 C_{10}\text{-Br}$. The C_{10} position in $C_9 C_{10}\text{-Br}$ is lightened to indicate occupational disorder. Gray, blue, and dark red spheres correspond to C, N, and Br atoms, respectively, while H atoms are omitted for clarity.

with short chains and long chains pack with long chains. Despite adopting a different space group (orthorhombic, $Pnma$), the same packing arrangement is observed in C_2C_{10} -Br, where the short chains (C_2 portions) pack exclusively with other short chains (Figure 3b). However, in the 100-K crystal structure of C_9C_{10} -Br (monoclinic, $C2$), a different picture emerges: in this salt, occupational disorder at the C_{10} position of both alkyl chains—50:50 when constrained into the higher symmetry space group $C2$, and 47(2):53(2) if unconstrained in the lower symmetry space group $P1$ —suggests that the C_9 portions on one $[C_9C_{10}]^+$ cation pack indiscriminately with C_9 or C_{10} portions on adjacent $[C_9C_{10}]^+$ cations (Figure 3c). Otherwise, the structure for C_9C_{10} -Br is very similar to that of $C_{10}C_{10}$ -Br with respect to chain confinement areas and dihedral angles (Table S2).

In the absence of ordered phase crystal structures for the full C_mC_{10} -Br series, we turned to powder X-ray diffraction (PXRD) for further structural insight, as all salts are crystalline in both their low-temperature and high-temperature phases. Evenly spaced Bragg peaks at low angles were observed in all diffraction patterns, confirming that all salts adopt lamellar structures (Figures S37–S45).²⁹ Next, for a given salt, unit cell parameters for the ordered phase (relative to the lowest transition temperature) were obtained by performing structureless Le Bail refinements on PXRD patterns. From these refinements, we found that the lengths of the hydrocarbon chain axis and unit cell volumes follow a linear trend with increasing m (Figure S46 and Table S4). These results suggest that across the series, the ordered phases of C_mC_{10} -Br salts maintain a noninterdigitated packing arrangement, as the adoption of an interdigitated structure would result in a decrease in the hydrocarbon chain axis length.^{34,35} The insights obtained from crystal structures and unit cell parameters lead us to tentatively hypothesize that there are two competing effects contributing to the caldera-like behavior in C_mC_{10} -Br transition temperatures. First, we speculate that the non-interdigitated, end-to-end packing arrangement observed in C_9C_{10} -Br—where long and short chains pack together in a disordered fashion—could also be present for other intermediate chain lengths. This disordered packing, in turn, could be responsible for some of the transition temperature decreases that are observed, similar to how mixing hydrocarbon chains of different lengths in pure hydrocarbon solids leads to melting temperature depression, in part by disrupting the uniformity of van der Waals interactions.^{36,37} Second, an increased average hydrocarbon chain length should favor a higher transition temperature,³⁸ which could account for the increasing transition temperatures observed for $m = 6$ and above.

Barocaloric Properties of Asymmetric Dialkylammonium (C_mC_{10} -Br) Salts. Owing to the substantial pressure-induced thermal changes accessible in symmetric dialkylammonium salts,^{14,15,22} we anticipated that asymmetric dialkylammonium salts could also exhibit favorable barocaloric properties. For barocaloric applications, materials in which large entropy changes are accessible across a single transition are generally more desirable than materials in which entropy changes are distributed over several transitions.¹³ As such, we focused on assessing barocaloric parameters for only the C_mC_{10} -Br salts that undergo highly reproducible, single transitions: C_1C_{10} -Br, C_2C_{10} -Br, C_8C_{10} -Br, and C_9C_{10} -Br. Nonetheless, the thermal phase-change behavior for C_3C_{10} -Br through C_7C_{10} -Br—all of which exhibit multiple

transitions, or, in the case of C_4C_{10} -Br, undergo a transition that is highly sensitive to the specific sample crystallization conditions and thermal scan rate (Figures S74–S78)—is summarized in Tables S6–S8.

Having narrowed the materials space to C_1C_{10} -Br, C_2C_{10} -Br, C_8C_{10} -Br, and C_9C_{10} -Br, we first assessed the magnitudes of their respective phase transition entropy changes (ΔS_{tr}), which sets the upper limit of the amount of heat able to be moved through the phase transition. Specifically, ΔS_{tr} values (Figure 4, top) were determined by integrating the heat flow

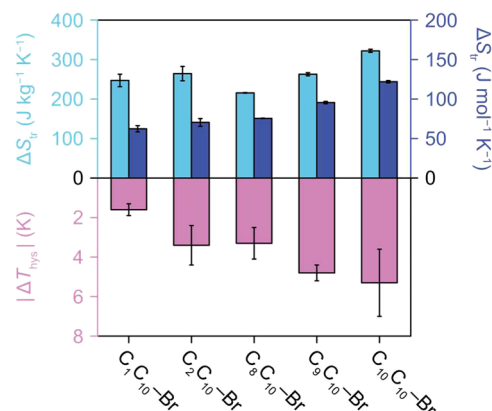


Figure 4. Phase transition entropy changes (ΔS_{tr}) and associated (onset) thermal hysteresis (ΔT_{hys}) in C_mC_{10} -Br salts that undergo single, reproducible chain-melting transitions. Error bars were determined from triplicate measurements.

data (collected on 3–5 mg of sample at a scan rate of 2 K/min) for a given transition at ambient pressure and dividing by the associated heating transition (onset) temperature. On a molar basis, C_1C_{10} -Br undergoes an entropy change nearly half that of $C_{10}C_{10}$ -Br (62 and 122 J mol⁻¹ K⁻¹, respectively), suggesting that the methyl group in C_1C_{10} -Br contributes little appreciable disordering to the phase transition. However, as the m chain length grows from C_2C_{10} -Br to C_9C_{10} -Br, so too does the corresponding molar entropy change—a trend consistent with a longer chain contributing additional disordering to the phase transition. Meanwhile, on a gravimetric basis, all four materials possess large ΔS_{tr} values exceeding 200 J kg⁻¹ K⁻¹.

In addition to entropy changes, the degree of thermal hysteresis (ΔT_{hys}) associated with the phase transition also has a critical impact on barocaloric performance, since thermal hysteresis substantially increases the pressure required to drive phase transitions in a reversible fashion.³⁹ For C_1C_{10} -Br, C_2C_{10} -Br, C_8C_{10} -Br, and C_9C_{10} -Br, ΔT_{hys} values were extracted from DSC traces (collected on 3–5 mg of sample at a scan rate of 2 K/min) as the difference between onset temperatures on heating and cooling (Figure 4, bottom). All four asymmetric salts exhibit lower hysteresis than the fully symmetric $C_{10}C_{10}$ -Br, which possesses a ΔT_{hys} of nearly 6 K. Of particular note is C_1C_{10} -Br, which possesses a ΔT_{hys} of around 1.6 K—one of the lowest thermal hysteresis values reported to date for dialkylammonium salts, symmetric or asymmetric.^{14,15,21,22} More generally, we note that the range of onset ΔT_{hys} values observed for these asymmetric dialkylammonium salts ($\Delta T_{hys} = 1.6$ K–4.8 K) is lower than—or comparable to—the ranges of heating onset-to-cooling onset and peak-to-peak thermal hysteresis observed in other high-

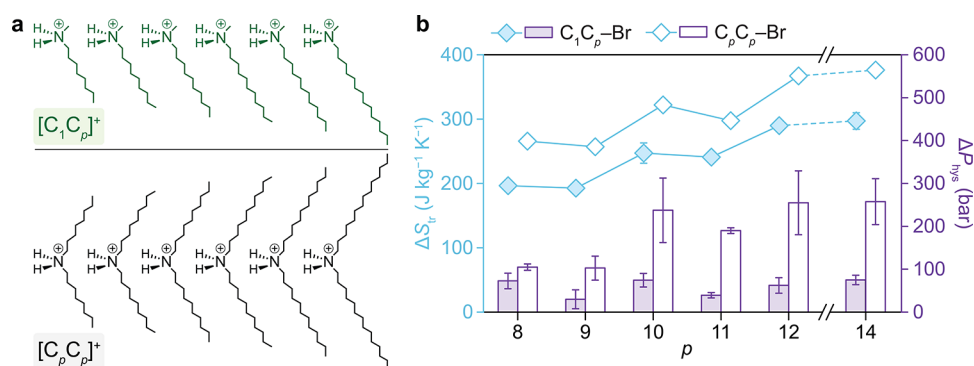


Figure 5. (a) ChemDraw representations of $[C_1C_p]^+$ (dark green) and $[C_pC_p]^+$ (black) dialkylammonium cations for $p = 8, 9, 10, 11, 12,$ and 14 . (b) Phase transition entropy changes (ΔS_p) and pressure hysteresis (ΔP_{hys}) for asymmetric $C_1C_p\text{-Br}$ salts (filled diamonds and bars) compared to their symmetric $C_pC_p\text{-Br}$ counterparts (unfilled diamonds and bars). Note that some error bars (determined from triplicate measurements) are smaller than the size of the data points.

entropy barocaloric materials, such as plastic crystals ($\Delta T_{\text{hys, onset}} = 3.7 \text{ K} - 76 \text{ K}$)^{7,39} and hybrid organic–inorganic perovskites ($\Delta T_{\text{hys, peak}} = 0.9 \text{ K} - 7 \text{ K}$).^{13,40,41} Of the four asymmetric salts evaluated here, $C_1C_{10}\text{-Br}$ represents a particularly promising barocaloric material due to its low hysteresis and high entropy change.

Low Pressure Hysteresis in a Subset of Asymmetric Dialkylammonium ($C_1C_p\text{-Br}$) Salts. To investigate whether the low hysteretic behavior observed in $C_1C_{10}\text{-Br}$ was a unique phenomenon or could be generalized to a wider range of materials, we synthesized a new series of asymmetric dialkylammonium salts of the form $C_1C_p\text{-Br}$, where one alkyl substituent is fixed as a methyl group while the other varies in length from $p = 8$ to 14 (Figure 5a). All $C_1C_p\text{-Br}$ salts were observed by DSC to undergo single, reversible chain-melting transitions between 298 and 350 K. With increasing p values, the phase transition temperature increases in a staggered fashion—similar to the odd–even melting point alternation observed for n -alkyl-containing systems^{42,43}—suggesting that lower or higher phase transition temperatures can be predictably accessed in $C_1C_p\text{-Br}$ salts beyond $p = 8-14$.

All associated ΔT_{hys} values for these compounds were found to be less than or equal to 2 K (Table S9). Excitingly, the consistent observation of low thermal hysteresis in the $C_1C_p\text{-Br}$ series suggests that the highly asymmetric $[C_1C_p]^+$ cation can be used as a template for endowing dialkylammonium salts with reduced hysteresis. Several hypotheses have been advanced regarding the origins of hysteresis in caloric materials—most notably for shape-memory alloys, but also more recently for plastic crystals—with an emphasis on the nucleation and growth mechanisms that govern their (often first-order) solid–solid phase transitions. For instance, in shape-memory alloys, hysteresis has been linked to a stressed transition layer between ordered and disordered phases.⁴⁴ Efforts to minimize strain at this interface—such as by tuning alloy composition to increase geometric phase compatibility—have successfully reduced hysteresis in a variety of shape-memory alloys.^{45,46} Meanwhile, recent investigations into thermal hysteresis in organic plastic crystals have found that nucleation of the dynamically disordered phase plays a significant role in dictating the extent of supercooling—and thereby hysteresis—observed.^{47,48} These findings suggest that lowering the energetic barrier(s) to nucleation events may promote reduced hysteresis in rotationally disordered systems.

For our dialkylammonium materials, we tentatively hypothesize that the low hysteresis observed in $C_1C_p\text{-Br}$ compounds is related to the C_1/C_1 interface—which likely remains relatively constant across the phase transition, as suggested by the lack of a molar entropy change contribution from the C_1 portion in $C_1C_{10}\text{-Br}$ —increasing compatibility between the ordered and disordered phases and thereby decreasing the barrier to nucleation and/or propagation of the ordering phase transition. Potential mechanisms by which the C_1/C_1 interface may promote phase transition reversibility include (i) the relatively low barrier to rotation of methyl groups favoring nucleation at the C_1/C_1 interface (as opposed to the symmetric $C_{10}C_{10}\text{-Br}$ salt, in which nucleation at the C_{10}/C_{10} interface would involve ordering of larger decyl groups), or (ii) minimization of lattice strain through decreased interfacial strain at phase boundaries (as has been reported for martensitic transformations⁴⁴). Efforts to interrogate the intrinsic and extrinsic mechanisms that drive the low hysteretic behavior in asymmetric $C_1C_p\text{-Br}$ salts compared to symmetric $C_pC_p\text{-Br}$ salts will be the subject of future optical microscopy and calorimetry studies in our laboratory.

Low ΔT_{hys} values have important implications for ΔP_{hys} , or pressure hysteresis, which represents the minimum pressure needed to reversibly access nonzero isothermal entropy changes in a barocaloric material. Specifically, ΔP_{hys} is related to ΔT_{hys} by $\Delta P_{\text{hys}} = \frac{\Delta T_{\text{hys}}}{dT/dP}$, where dT/dP represents the barocaloric coefficient, or pressure sensitivity of the phase transition temperature during cooling.⁴⁹ As such, to evaluate the potential benefits of low ΔT_{hys} for reducing ΔP_{hys} , we first obtained dT/dP values for $C_1C_p\text{-Br}$ and $C_pC_p\text{-Br}$ salts by conducting high-pressure DSC (HP-DSC) experiments using a He pressure-transmitting medium up to 150 bar (Figures S89–S97). Promisingly, asymmetric and symmetric salts exhibit similar pressure sensitivities—with average dT/dP values ranging from 18 to 23 K kbar⁻¹ for $C_1C_p\text{-Br}$ salts and from 20 to 26 K kbar⁻¹ for $C_pC_p\text{-Br}$ salts (Table S10)—suggesting that the pressure hysteresis for these materials should be directly impacted by the magnitude of ΔT_{hys} . Indeed, the advantages afforded by low ΔT_{hys} values become especially pronounced when comparing ΔP_{hys} values between the highly asymmetric $C_1C_p\text{-Br}$ salts and their symmetric $C_pC_p\text{-Br}$ counterparts (Figure 5b). For each p value investigated, $C_1C_p\text{-Br}$ salts consistently feature lower pressure hysteresis compared to $C_pC_p\text{-Br}$ salts, with reductions in ΔP_{hys} ranging from 31%

($p = 8$) to as much as 76% ($p = 11$). Moreover, to verify the magnitudes of calculated ΔP_{hys} values, we calculated isothermal, pressure-induced entropy changes for $C_1C_{10}\text{-Br}$ (Figure S100) and found that the pressure range corresponding to nonzero overlap of isothermal entropy curves agrees with the magnitude of ΔP_{hys} .

These sizable reductions in pressures are accompanied by only moderate decreases in phase transition entropy changes—a trade-off that is consistent with $C_1C_p\text{-Br}$ salts possessing a lower mass fraction of carbon atoms that participate in the chain-melting transition than their $C_pC_p\text{-Br}$ analogues. Even so, $C_1C_p\text{-Br}$ salts are able to access 74–81% of the ΔS_{tr} of their $C_pC_p\text{-Br}$ analogues on a gravimetric basis. Taken together, the large phase transition entropy changes and low pressure hysteresis displayed by asymmetric $C_1C_p\text{-Br}$ salts distinguish this subset of dialkylammonium salts from their more symmetric counterparts.

CONCLUSIONS

Hydrocarbon chain-melting processes constitute a promising class of solid–solid phase transitions to exploit for barocaloric applications, yet the development of design principles to manipulate the thermodynamics and kinetics of chain melting is hindered by a relatively limited materials phase space. The asymmetric dialkylammonium salts reported here represent a new family of chain-melting materials with large entropy changes ($\Delta S_{\text{tr}} > 200 \text{ J kg}^{-1} \text{ K}^{-1}$) and low hysteresis ($\Delta T_{\text{hys}} < 5 \text{ K}$). Moreover, chain length desymmetrization provides a generalizable strategy for reducing thermal hysteresis while maintaining high entropy changes and sharp phase transitions. Ultimately, this work illustrates an approach to modulate chain-melting transitions through direct, synthetic modification of alkyl chains; expands the existing phase space of chain-melting materials; and advances several, newly reported asymmetric dialkylammonium salts as promising barocaloric materials. Future investigations into the intrinsic and extrinsic mechanisms underlying the low hysteresis observed in methyl- n -alkylammonium salts should yield even more insight into the nature of chain-melting transitions.

ASSOCIATED CONTENT

Supporting Information

The Supporting Information is available free of charge at <https://pubs.acs.org/doi/10.1021/jacs.5c03705>.

Additional experimental details; synthetic methods; ^1H and $^{13}\text{C}\{^1\text{H}\}$ NMR spectra; ESI-MS spectra; single-crystal and powder X-ray diffraction data; thermogravimetric analysis; and calorimetry data (PDF)

Accession Codes

Deposition Numbers 2424654–2424657 contain the supplementary crystallographic data for this paper. These data can be obtained free of charge via the joint Cambridge Crystallographic Data Centre (CCDC) and Fachinformationszentrum Karlsruhe [Access Structures service](#).

AUTHOR INFORMATION

Corresponding Author

Jarad A. Mason – Department of Chemistry and Chemical Biology, Harvard University, Cambridge, Massachusetts 02138, United States; orcid.org/0000-0003-0328-7775; Email: mason@chemistry.harvard.edu

Authors

- Faith E. Chen – Department of Chemistry and Chemical Biology, Harvard University, Cambridge, Massachusetts 02138, United States; orcid.org/0000-0003-2230-6257
- Jason D. Braun – Department of Chemistry and Chemical Biology, Harvard University, Cambridge, Massachusetts 02138, United States; orcid.org/0000-0002-5850-8048
- Jinyoung Seo – Department of Chemistry and Chemical Biology, Harvard University, Cambridge, Massachusetts 02138, United States; orcid.org/0000-0002-3260-4963
- Hailey J. Hurd – Department of Chemistry and Chemical Biology, Harvard University, Cambridge, Massachusetts 02138, United States; orcid.org/0000-0002-9139-8864
- Malia B. Wenny – NIST Center for Neutron Research, National Institute of Standards and Technology, Gaithersburg, Maryland 20899, United States; orcid.org/0000-0002-0704-8184
- Shao-Liang Zheng – Department of Chemistry and Chemical Biology, Harvard University, Cambridge, Massachusetts 02138, United States; orcid.org/0000-0002-6432-9943
- Jason J. Calvin – Department of Chemistry and Chemical Biology, Harvard University, Cambridge, Massachusetts 02138, United States; orcid.org/0000-0001-8381-2466
- Craig M. Brown – NIST Center for Neutron Research, National Institute of Standards and Technology, Gaithersburg, Maryland 20899, United States; orcid.org/0000-0002-9637-9355

Complete contact information is available at:

<https://pubs.acs.org/doi/10.1021/jacs.5c03705>

Notes

The authors declare the following competing financial interest(s): J.S., F.E.C., J.D.B., and J.A.M. are inventors of technology utilized in this research that is licensed to PasCal Technologies, Inc., of which J.S. and J.A.M. are co-founders. By improving upon the licensed technology, the outcomes of this research could result in a financial benefit to J.S., F.E.C., J.D.B., and J.A.M., and PasCal Technologies, Inc.

ACKNOWLEDGMENTS

We acknowledge support from the National Science Foundation through the Harvard MRSEC program (DMR-2011754) and a Graduate Research Fellowship awarded to F.E.C. Single-crystal X-ray diffraction experiments made use of the Harvard X-ray Core Facility, for which we acknowledge support from the Major Research Instrumentation (MRI) Program of the National Science Foundation under Award Number 2216066. We thank Dr. Hui Zhong for technical assistance with synchrotron powder X-ray diffraction experiments conducted at beamline 28-ID-2 at the National Synchrotron Light Source II, a U.S. Department of Energy (DOE) Office of Science User Facility operated for the DOE Office of Science by Brookhaven National Laboratory under Contract No. DE-SC0012704. Synchrotron powder X-ray diffraction at Beamline 28-ID-2 was also supported by the NIST Center for Neutron Research. Certain commercial equipment, instruments, or materials are identified in this document. Such identification does not imply recommendation or endorsement by the National Institute of Standards and Technology, nor does it imply that the products identified are necessarily the best available for the purpose. The views expressed in the article do not necessarily represent the views

of the DOE or the U.S. Government. The U.S. Government retains, and the publisher, by accepting the article for publication, acknowledges that the U.S. Government retains a nonexclusive, paid-up, irrevocable, worldwide license to publish or reproduce the published form of this work, or allow others to do so, for U.S. Government purposes. We also thank Dr. Andrey Yakovenko for technical assistance with synchrotron powder X-ray diffraction experiments conducted at beamline 17-BM at the Advanced Photon Source at Argonne National Laboratory, which is supported by the U.S. Department of Energy, Office of Science, Office of Basic Energy Sciences under Contract No. DE-AC02-06CH11357. We thank Dr. Daniel Laorenza for valuable scientific discussions, as well as Prof. Danna Freedman's Group for use of their Physical Properties Measurement System.

REFERENCES

- (1) Moya, X.; Mathur, N. D. Caloric Materials for Cooling and Heating. *Science* **2020**, *370* (6518), 797–803.
- (2) Mañosa, L.; Planes, A. Solid-State Cooling by Stress: A Perspective. *Appl. Phys. Lett.* **2020**, *116* (5), No. 050501.
- (3) McCulloch, A. Fluorocarbons in the Global Environment: A Review of the Important Interactions with Atmospheric Chemistry and Physics. *J. Fluorine Chem.* **2003**, *123* (1), 21–29.
- (4) Velders, G. J. M.; Daniel, J. S.; Montzka, S. A.; Vimont, I.; Rigby, M.; Krummel, P. B.; Muhle, J.; O'Doherty, S.; Prinn, R. G.; Weiss, R. F.; Young, D. Projections of Hydrofluorocarbon (HFC) Emissions and the Resulting Global Warming Based on Recent Trends in Observed Abundances and Current Policies. *Atmos. Chem. Phys.* **2022**, *22* (9), 6087–6101.
- (5) McGillen, M. R.; Fried, Z. T. P.; Khan, M. A. H.; Kuwata, K. T.; Martin, C. M.; O'Doherty, S.; Pecere, F.; Shallcross, D. E.; Stanley, K. M.; Zhang, K. Ozonolysis Can Produce Long-Lived Greenhouse Gases from Commercial Refrigerants. *Proc. Natl. Acad. Sci. U.S.A.* **2023**, *120* (51), No. e2312714120.
- (6) Boldrin, D. Fantastic Barocalorics and Where to Find Them. *Appl. Phys. Lett.* **2021**, *118* (17), No. 170502.
- (7) Loveras, P.; Aznar, A.; Barrio, M.; Negrier, Ph.; Popescu, C.; Planes, A.; Mañosa, L.; Stern-Taulats, E.; Avramenko, A.; Mathur, N. D.; Moya, X.; Tamarit, J.-L. Colossal Barocaloric Effects near Room Temperature in Plastic Crystals of Neopentylglycol. *Nat. Commun.* **2019**, *10* (1), No. 1803.
- (8) Li, B.; Kawakita, Y.; Ohira-Kawamura, S.; Sugahara, T.; Wang, H.; Wang, J.; Chen, Y.; Kawaguchi, S. I.; Kawaguchi, S.; Ohara, K.; Li, K.; Yu, D.; Mole, R.; Hattori, T.; Kikuchi, T.; Yano, S.; Zhang, Z.; Zhang, Z.; Ren, W.; Lin, S.; Sakata, O.; Nakajima, K.; Zhang, Z. Colossal Barocaloric Effects in Plastic Crystals. *Nature* **2019**, *567* (7749), 506–510.
- (9) McLinden, M. O. *Thermophysical Properties of Refrigerants*; ASHRAE, 2009.
- (10) Guillaume, F.; Coddens, G.; Dianoux, A. J.; Petry, W.; Rey-Lafon, M.; Sourisseau, C. Molecular Motions of Decylammonium Chains in the Perovskite Type Layered Compound $(C_{10}H_{21}NH_3)_2MnCl_4$: An Incoherent Neutron Scattering Study. *Mol. Phys.* **1989**, *67* (3), 665–679.
- (11) Kind, R.; Pleko, S.; Arend, H.; Blinc, R.; Seliger, J.; Loar, B.; Slak, J.; Levstik, A.; Filipi, C.; Lahajnar, G.; Milia, F.; Chapuis, G. Dynamics of the N-Decylammonium Chains in the Perovskite-Type Layer Structure Compound $(C_{10}H_{21}NH_3)_2CdCl_4$. *J. Chem. Phys.* **1979**, *71* (5), 2118.
- (12) Li, J.; Barrio, M.; Dunstan, D. J.; Dixey, R.; Lou, X.; Tamarit, J.; Phillips, A. E.; Lloveras, P. Colossal Reversible Barocaloric Effects in Layered Hybrid Perovskite $(C_{10}H_{21}NH_3)_2MnCl_4$ under Low Pressure Near Room Temperature. *Adv. Funct. Mater.* **2021**, *31* (46), No. 2105154.
- (13) Seo, J.; McGillicuddy, R. D.; Slavney, A. H.; Zhang, S.; Ukani, R.; Yakovenko, A. A.; Zheng, S.-L.; Mason, J. A. Colossal Barocaloric Effects with Ultralow Hysteresis in Two-Dimensional Metal–Halide Perovskites. *Nat. Commun.* **2022**, *13* (1), No. 2536.
- (14) Seo, J.; Ukani, R.; Zheng, J.; Braun, J. D.; Wang, S.; Chen, F. E.; Kim, H. K.; Zhang, S.; Thai, C.; McGillicuddy, R. D.; Yan, H.; Vlassak, J. J.; Mason, J. A. Barocaloric Effects in Dialkylammonium Halide Salts. *J. Am. Chem. Soc.* **2024**, *146* (4), 2736–2747.
- (15) Gao, Y.-H.; Wang, D.-H.; Hu, F.-X.; Huang, Q.-Z.; Song, Y.-T.; Yuan, S.-K.; Tian, Z.-Y.; Wang, B.-J.; Yu, Z.-B.; Zhou, H.-B.; Kan, Y.; Lin, Y.; Wang, J.; Li, Y.; Liu, Y.; Chen, Y.-Z.; Sun, J.-R.; Zhao, T.-Y.; Shen, B.-G. Low Pressure Reversibly Driving Colossal Barocaloric Effect in Two-Dimensional vdW Alkylammonium Halides. *Nat. Commun.* **2024**, *15* (1), No. 1838.
- (16) Yao, Y.; Cao, D.; Yan, J.; Zhang, M.; Chen, X.; Shu, H. Spacer Cation Engineering of Two-Dimensional Hybrid Perovskites with Tunable Band Alignment and Optoelectronic Properties. *J. Phys. Chem. C* **2022**, *126* (19), 8408–8416.
- (17) Guo, S.; Mihalyi-Koch, W.; Mao, Y.; Li, X.; Bu, K.; Hong, H.; Hautzinger, M. P.; Luo, H.; Wang, D.; Gu, J.; Zhang, Y.; Zhang, D.; Hu, Q.; Ding, Y.; Yang, W.; Fu, Y.; Jin, S.; Lü, X. Exciton Engineering of 2D Ruddlesden–Popper Perovskites by Synergistically Tuning the Intra and Interlayer Structures. *Nat. Commun.* **2024**, *15* (1), No. 3001.
- (18) Kingsford, R. L.; Jackson, S. R.; Bloxham, L. C.; Bischak, C. G. Controlling Phase Transitions in Two-Dimensional Perovskites through Organic Cation Alloying. *J. Am. Chem. Soc.* **2023**, *145*, No. jacs.3c02956.
- (19) van Oort, M. J. M.; White, M. A. Polymorphism in Dialkylammonium Chlorides. An Adiabatic Calorimetry Study. *Ber. Bunsenges. Phys. Chem.* **1988**, *92* (2), 168–176.
- (20) Whitman, C. A.; Johnson, M. B.; White, M. A. Characterization of Thermal Performance of a Solid–Solid Phase Change Material, Din-Hexylammonium Bromide, for Potential Integration in Building Materials. *Thermochim. Acta* **2012**, *531*, 54–59.
- (21) Steinert, S.; Voigt, W.; Glausch, R.; Neuschütz, M. Thermal Characteristics of Solid–Solid Phase Transitions in Long-Chain Dialkyl Ammonium Salts. *Thermochim. Acta* **2005**, *435* (1), 28–33.
- (22) García-Ben, J.; Bermúdez-García, J. M.; Dixey, R. J. C.; Delgado-Ferreiro, I.; Llamas-Saiz, A. L.; López-Beceiro, J.; Artiaga, R.; García-Fernández, A.; Cappel, U. B.; Alonso, B.; Castro-García, S.; Phillips, A. E.; Sánchez-Andújar, M.; Señaris-Rodríguez, M. A. Structure and Thermal Property Relationships in the Thermomaterial Di-*n*-Butylammonium Tetrafluoroborate for Multipurpose Cooling and Cold-Storage. *J. Mater. Chem. A* **2023**, *11* (41), 22232–22247.
- (23) Koynova, R.; Caffrey, M. Phases and Phase Transitions of the Phosphatidylcholines. *Biochim. Biophys. Acta, Rev. Biomembr.* **1998**, *1376* (1), 91–145.
- (24) Kahwaji, S.; White, M. A. Organic Phase Change Materials for Thermal Energy Storage: Influence of Molecular Structure on Properties. *Molecules* **2021**, *26* (21), No. 6635.
- (25) Schaerer, A. A.; Busso, C. J.; Smith, A. E.; Skinner, L. B. Properties of Pure Normal Alkanes in the C_{17} to C_{36} Range. *J. Am. Chem. Soc.* **1955**, *77* (7), 2017–2019.
- (26) Broadhurst, M. G. An Analysis of the Solid Phase Behavior of the Normal Paraffins. *J. Res. Natl. Bur. Stand., Sect. A* **1962**, *66A* (3), 241.
- (27) Huang, C. Mixed-chain Phospholipids: Structures and Chain-melting Behavior. *Lipids* **2001**, *36* (10), 1077–1097.
- (28) Lin, H.-n.; Wang, Z.; Huang, C. The Influence of Acyl Chain-Length Asymmetry on the Phase Transition Parameters of Phosphatidylcholine Dispersions. *Biochim. Biophys. Acta, Biomembr.* **1991**, *1067* (1), 17–28.
- (29) Mattai, J.; Sripada, P. K.; Shipley, G. G. Mixed-Chain Phosphatidylcholine Bilayers: Structure and Properties. *Biochemistry* **1987**, *26* (12), 3287–3297.
- (30) McIntosh, T. J.; Simon, S. A.; Ellington, J. C.; Porter, N. A. New Structural Model for Mixed-Chain Phosphatidylcholine Bilayers. *Biochemistry* **1984**, *23* (18), 4038–4044.
- (31) Lewis, R. N.; McElhaney, R. N. Studies of Mixed-Chain Diacyl Phosphatidylcholines with Highly Asymmetric Acyl Chains: A Fourier

Transform Infrared Spectroscopic Study of Interfacial Hydration and Hydrocarbon Chain Packing in the Mixed Interdigitated Gel Phase. *Biophys. J.* **1993**, *65* (5), 1866–1877.

(32) Lewis, R. N.; McElhaney, R. N.; Monck, M. A.; Cullis, P. R. Studies of Highly Asymmetric Mixed-Chain Diacyl Phosphatidylcholines That Form Mixed-Interdigitated Gel Phases: Fourier Transform Infrared and ²H NMR Spectroscopic Studies of Hydrocarbon Chain Conformation and Orientational Order in the Liquid-Crystalline State. *Biophys. J.* **1994**, *67* (1), 197–207.

(33) Huang, C.; Mason, J. T.; Levin, I. W. Raman Spectroscopic Study of Saturated Mixed-Chain Phosphatidylcholine Multilamellar Dispersions. *Biochemistry* **1983**, *22* (11), 2775–2780.

(34) Hui, S. W.; Mason, J. T.; Huang, C. Acyl Chain Interdigitation in Saturated Mixed-Chain Phosphatidylcholine Bilayer Dispersions. *Biochemistry* **1984**, *23* (23), 5570–5577.

(35) Abdallah, D. J.; Robertson, A.; Hsu, H.-F.; Weiss, R. G. Smectic Liquid-Crystalline Phases of Quaternary Group VA (Especially Phosphonium) Salts with Three Equivalent Long *n*-Alkyl Chains. How Do Layered Assemblies Form in Liquid-Crystalline and Crystalline Phases? *J. Am. Chem. Soc.* **2000**, *122* (13), 3053–3062.

(36) Orwoll, R. A.; Flory, P. J. Thermodynamic Properties of Binary Mixtures of *N*-Alkanes. *J. Am. Chem. Soc.* **1967**, *89* (26), 6822–6829.

(37) Maroncelli, M.; Strauss, H. L.; Snyder, R. G. Structure of the *N*-Alkane Binary Solid *n*-C₁₉H₄₀/*n*-C₂₁H₄₄ by Infrared Spectroscopy and Calorimetry. *J. Phys. Chem. A* **1985**, *89* (24), 5260–5267.

(38) Takamizawa, K.; Ogawa, Y.; Oyama, T. Thermal Behavior of *N*-Alkanes from *n*-C₃₂H₆₆ to *n*-C₈₀H₁₆₂, Synthesized with Attention Paid to High Purity. *Polym. J.* **1982**, *14* (6), 441–456.

(39) Aznar, A.; Lloveras, P.; Barrio, M.; Negrier, P.; Planes, A.; Mañosa, L.; Mathur, N. D.; Moya, X.; Tamarit, J.-L. Reversible and Irreversible Colossal Barocaloric Effects in Plastic Crystals. *J. Mater. Chem. A* **2020**, *8* (2), 639–647.

(40) Bermúdez-García, J. M.; Yáñez-Vilar, S.; García-Fernández, A.; Sánchez-Andújar, M.; Castro-García, S.; López-Beceiro, J.; Artiaga, R.; Dilshad, M.; Moya, X.; Señaris-Rodríguez, M. A. Giant Barocaloric Tunability in [(CH₃ CH₂ CH₂)₄ N]Cd[N(CN)₂]₃ Hybrid Perovskite. *J. Mater. Chem. C* **2018**, *6* (37), 9867–9874.

(41) Bermúdez-García, J. M.; Sánchez-Andújar, M.; Castro-García, S.; López-Beceiro, J.; Artiaga, R.; Señaris-Rodríguez, M. A. Giant Barocaloric Effect in the Ferroic Organic-Inorganic Hybrid [TPrA]-[Mn(Dca)₃] Perovskite under Easily Accessible Pressures. *Nat. Commun.* **2017**, *8* (1), No. 15715.

(42) McBride, J. M.; Bertman, S. B. Understanding Long-Chain Melting Points, Fritz Breusch, and Interface Thermodynamics. *Isr. J. Chem.* **2017**, *57* (1–2), 137–153.

(43) Thalladi, V. R.; Boese, R.; Weiss, H.-C. The Melting Point Alternation in α,ω -Alkanedithiols. *J. Am. Chem. Soc.* **2000**, *122* (6), 1186–1190.

(44) Song, Y.; Chen, X.; Dabade, V.; Shield, T. W.; James, R. D. Enhanced Reversibility and Unusual Microstructure of a Phase-Transforming Material. *Nature* **2013**, *502* (7469), 85–88.

(45) Zarnetta, R.; Takahashi, R.; Young, M. L.; Savan, A.; Furuya, Y.; Thienhaus, S.; Maaß, B.; Rahim, M.; Frenzel, J.; Brunken, H.; Chu, Y. S.; Srivastava, V.; James, R. D.; Takeuchi, I.; Eggeler, G.; Ludwig, A. Identification of Quaternary Shape Memory Alloys with Near-Zero Thermal Hysteresis and Unprecedented Functional Stability. *Adv. Funct. Mater.* **2010**, *20* (12), 1917–1923.

(46) Srivastava, V.; Chen, X.; James, R. D. Hysteresis and Unusual Magnetic Properties in the Singular Heusler Alloy Ni₄5C-₀5Mn₄₀Sn₁₀. *Appl. Phys. Lett.* **2010**, *97* (1), No. 014101.

(47) Somodi, C. B.; McCormick, K.; Tabor, D. P.; Pentzer, E.; Shamberger, P. J. Kinetics of the Plastic Crystal Transition in Neopentyl Glycol. *J. Appl. Phys.* **2024**, *135* (14), No. 145101.

(48) Rendell-Bhatti, F.; Boldrin, D.; Dilshad, M.; Moya, X.; MacLaren, D. A. Understanding Variations of Thermal Hysteresis in Barocaloric Plastic Crystal Neopentyl Glycol Using Correlative Microscopy and Calorimetry. *J. Phys. Energy* **2024**, *6* (2), No. 025020.

(49) Seo, J.; Braun, J. D.; Dev, V. M.; Mason, J. A. Driving Barocaloric Effects in a Molecular Spin-Crossover Complex at Low Pressures. *J. Am. Chem. Soc.* **2022**, *144* (14), 6493–6503.